

Deformation of a laser beam in the fabrication of graphite microstructures inside a volume of diamond

T.V. Kononenko, E.V. Zavedeev

Abstract. We report a theoretical and experimental study of the energy profile deformation along the laser beam axis during the fabrication of graphite microstructures inside a diamond crystal. The numerical simulation shows that the use of a focusing lens with a numerical aperture $NA < 0.1$ at a focusing depth of up to 2 mm makes it possible to avoid a noticeable change in the energy profile of the beam due to the spherical aberration that occurs in the case of refraction of the focused laser beam at the air – diamond interface. The calculation results are confirmed by experimental data on the distribution of the laser intensity along the beam axis in front of its focal plane, derived from observations of graphitisation wave propagation in diamond. The effect of radiation self-focusing on laser-induced graphitisation of diamond is analysed. It is shown that if the wavefront distortion due to self-focusing can be neglected at a minimum pulse energy required for the optical breakdown of diamond, then an increase in the beam distortion with increasing pulse energy has no effect on the graphitisation process.

Keywords: laser, diamond, spherical aberration, self-focusing.

1. Introduction

Femtosecond laser pulses allow local modification of the structure and properties of some transparent materials, paving the way for the fabrication of various miniature devices in their volume for integrated optics and other applications, such as buried waveguides [1], couplers [2], directional couplers [3], waveguide lasers [4], 3D microchannels [5], etc. One of the known problems of this technology is the spherical aberration that occurs during refraction of the focused laser beam on a plane front surface of an irradiated sample [6, 7]. The wavefront distortion leads to a decrease in the maximum intensity of the focused beam and a lengthening of the caustic, the effect becoming stronger with extending the focal spot region into the sample [8]. With respect to the waveguides written by a laser inside glass, when the scanning direction is perpendicular to the laser beam, it means progressive deformation of the waveguide cross section [9]. This effect can be significantly reduced by means of immersion oil that fills the gap between the objective and the sample, or by using a tun-

able ‘dry’ objective that can compensate for the spherical aberration for a certain range of focusing depths [10]. To write a waveguide with a circular cross section inside a glass plate, Diez-Blanco et al. [11] suggested using an elliptically shaped beam together with low numerical aperture optics [11].

The problem of spherical aberrations is also urgent for laser microstructuring in the volume of diamond. This technology has been actively developed in recent years [12–20] and is based on the local laser-induced transformation of diamond into graphite, which is accompanied by a radical change of the material properties. The effects of spherical aberration in diamond, when use is made of a high numerical aperture objective ($NA = 1.4$), were experimentally investigated in [15]. It was shown [15, 20] that the correction of the laser beam wavefront with the help of adaptive optics (a membrane deformable mirror and/or a liquid crystal spatial phase modulator) allows one to reduce dramatically spherical aberrations. However, it still remains unclear how much spherical aberrations affect the process of microstructuring of diamond in the case of using focusing optics with a lower numerical aperture that has been used in most other publications.

The present work is devoted to a theoretical and experimental study of the wavefront (deformation) distortion of laser beams focused by relatively low numerical aperture objectives ($NA = 0.09–0.36$) into diamond. The effect of spherical aberrations in diamond at a depth of 2 mm is simulated numerically, and its results are compared with experimental data on the intensity profile at the beam axis. The latter are obtained thanks to a unique feature of the process of laser microstructuring of diamond, namely the relationship between the local laser intensity and the graphitisation wave propagation velocity [21]. Comparison of the results for the laser pulses of different durations (140 fs – 15 ps) also makes it possible to evaluate the effect of self-focusing on the laser beam deformation.

2. Experiment

A plate measuring $5.2 \times 1.8 \times 1.1$ mm was cut from synthetic single crystal diamond grown in a microwave plasma (Innovative Plasma Systems GmbH). The four sides of the plate corresponding to $\{100\}$ and $\{110\}$ faces of the diamond crystal were mechanically polished using standard techniques. The diamond sample was irradiated with long trains of pulses ($\sim 10^4$ pulses) emitted by a Ti:sapphire laser (Spectra Physics) with a pulse repetition rate of 100 Hz at a wavelength $\lambda = 800$ nm. The tuning of the output compressor of the laser system allowed us to vary laser pulse duration within a small range: from 140 fs to 5 ps (FWHM of the autocorrelator signal). Using one of the two aspherical lens ($NA = 0.36$ or 0.09),

T.V. Kononenko, E.V. Zavedeev Natural Sciences Center, A.M. Prokhorov General Physics Institute, Russian Academy of Sciences, ul. Vavilova 38, 119991 Moscow, Russia; National Research Nuclear University ‘MEPhI’, Kashirskoe sh. 31, 115409 Moscow, Russia; e-mail: taras.kononenko@nsc.gpi.ru

Received 2 July 2015; revision received 18 January 2016
Kvantovaya Elektronika 46 (3) 229–235 (2016)

Translated by I.A. Ulitkin

the laser beam was focused inside the diamond plate to a depth from 70 μm to 1.7 mm. The focus position was not changed for the duration of the entire pulse train, but a new location on the sample was used for each irradiation cycle. The video surveillance system on the basis of a microscopic objective (20 \times) mounted perpendicular to the laser beam enabled real-time recording of the appearance and evolution of a graphitised area in diamond.

For both aspherical lenses we first studied focusing of the laser beam in the air. The target, which was a silicon wafer with a deposited thin film of amorphous carbon, was irradiated by single pulses with different energies. The size of the emerging ablation spots was measured using an optical microscope to obtain the dependence of the spot area S on the pulse energy logarithm Q . These measurements were repeated several times for different target positions of the target relative to the focal plane of the lens. In most cases the resulting dependences can be approximated by a linear function (lower inset in Fig. 1). This means that the radial profile of the energy density $F(r)$ corresponds to a Gaussian distribution: $F(r) = F_0 \exp(-r^2/w^2)$. Summing the results of measurements for various positions of the target on the optical axis (z axis), we found that the obtained dependence of the Gaussian radius w on coordinate obeys the known expression:

$$w(z) = w_0 \sqrt{1 + \frac{\lambda^2 z^2}{n^2 \pi^2 w_0^4}}, \quad (1)$$

where n is the refractive index of the medium, and w_0 is the minimal beam radius. The approximation by formula (1), which is shown in Fig. 1 by the dashed line, yields $w_0 = 0.67 \mu\text{m}$. Another well-known expression for the Gaussian beam determines the energy density distribution on the optical axis for a given pulse energy Q as follows:

$$F(z) = \frac{2Q}{\pi w^2(z)} = 2Q \left[\pi w_0^2 \left(1 + \frac{\lambda^2 z^2}{n^2 \pi^2 w_0^4} \right) \right]^{-1}. \quad (2)$$

It is important to emphasise that the absence of points on the dependence $w(z)$ near the focal plane ($z \in [-10 \mu\text{m}, 10 \mu\text{m}]$) in Fig. 1 is due to the nonlinear dependence of the spot area on the pulse energy logarithm in this region (top inset in

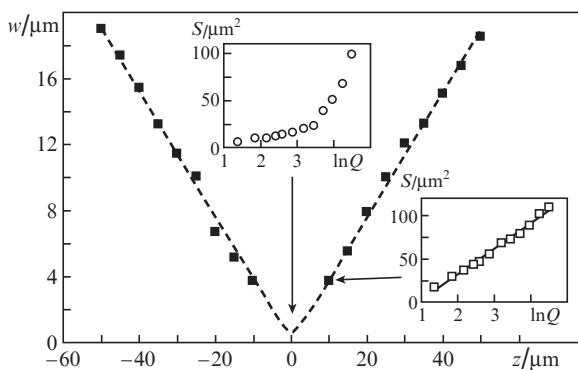


Figure 1. Coordinate dependence of the Gaussian radius (at the $1/e^2$ level) of the laser beam w , focused in the air with a lens having $\text{NA} = 0.36$. The dashed line shows the approximation of data by formula (1). The insets are the examples of the initial dependence of the ablation spot area S on the pulse energy logarithm Q , which is used to determine the Gaussian radius.

Fig. 1), rather than to a lack of experimental data. This behaviour is explained apparently by beam wavefront deformation in a high numerical aperture objective ($\text{NA} = 0.36$), which has a marked effect on the spatial intensity distribution only in the vicinity of the focal plane. The absence of noticeable deviations from the Gaussian distribution for a low numerical aperture objective ($\text{NA} = 0.09$), used in the experiments, indicates that the initial laser beam (before the focusing lens) is close to the TEM_{00} fundamental mode.

3. Processing of the experimental data

It is known that multi-pulse irradiation of a graphitised region which appears during the initial optical breakdown inside the diamond sample, causes a gradual extension of this region towards the laser beam, which can be described as the propagation of a graphitisation wave [12]. Experimental dependences of the graphitisation wave velocity on the coordinate for different pulse energies Q , obtained by computer processing of the video recording of the irradiation zone, were analysed in detail in [21]. It was shown that the instantaneous velocity of the graphitisation wave propagation can be represented as a sum of two components:

$$v(Q, z) = V_{\text{av}}(F(Q, z)) + \Delta(z), \quad (3)$$

where the first component is the average velocity determined by the local energy density, and the second component is a randomly fluctuating quantity. In [21], a method for an analysis of a large array of experimental data $v(Q, z)$ has also been proposed for several Q values, which can restore both the dependence of the average velocity on the energy density $[V_{\text{av}}(F)]$, and the distribution of the energy density on the beam axis $[F(Q, z)]$ before the intensity maximum under the condition that the local energy density is proportional to the pulse energy, i.e.

$$F(Q, z) = f(z)Q. \quad (4)$$

The result of data processing by this technique is shown in Fig. 2. The maximum energy density is achieved on the beam axis at point $z = 0$, located at a depth $d \approx 70 \mu\text{m}$ from the front surface of the diamond plate. As the graphitisation wave propagates towards the laser beam (i.e. from the right to the left) and moves away from the focal plane, the average propagation velocity of the wave is reduced until it complete stops. An increase in the laser pulse energy leads to the fact that both the place of optical breakdown and stopping point of the graphitisation wave shift towards the laser beam (to the left). The normalised energy profile of the focused beam $f(z)$ (upper left inset in Fig. 2) and the dependence of the wave velocity on the energy density $V_{\text{av}}(F)$ (upper right inset) are chosen so as to minimise the total deviation of the experimental points from the corresponding approximate curves $V_{\text{av}}(z)$.

Note that Fig. 2 shows the data related to only one series of measurements, while the total number of series was twenty. The series differed from one another by the value of one or more experimental parameters, including pulse duration τ , depth of focusing in diamond, numerical aperture of the focusing lens, and orientation of the crystal relative to the laser beam. Independent processing of each experimental series with a subsequent comparison of the recovered dependences $f(z)$ and $V_{\text{av}}(F)$ allowed us to verify the correctness and reliability of the technique in question. As was expected,

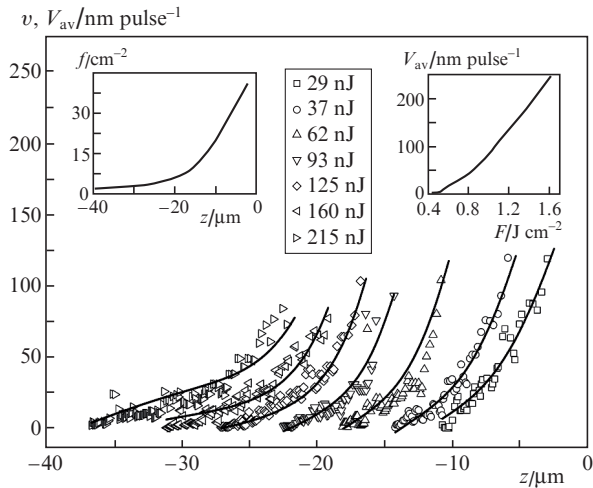


Figure 2. Experimental dependences of the graphitisation wave propagation velocity v on the coordinate for different pulse energies (points) ($\tau = 5$ ps, $\text{NA} = 0.36$, $d = 70$ μm). Fitting curves $V_{\text{av}}(z)$ (solid curves) for each energy are obtained from the recovered dependences of the wave velocity on the energy density $V_{\text{av}}(F)$ (upper right inset) and from the normalised energy density distribution on the beam axis $f(z)$ for $Q = 1$ μJ (upper left inset).

the dependence $V_{\text{av}}(F)$ was insensitive to changes in the focusing depth and numerical aperture if other parameters were fixed: local deviations of the recovered curves from the average did not exceed 5%. As will be shown below, the energy profile $f(z)$ could vary significantly in this case. At the same time, the recovered energy profile proved predictably independent of the pulse duration and crystal orientation.

Condition (4), which is the key in the recovery of the experimental power energy, is not fulfilled in the case of non-linear transformation of the propagating laser beam, particularly under the action of self-focusing. The critical self-focusing power [22] in diamond is $P_{\text{cr}} = \alpha\lambda^2/(4\pi n_0 n_2) \approx 810$ kW, where the geometric factor for a Gaussian beam is $\alpha = 1.9$, the linear refractive index is $n_0 = 2.4$, and the nonlinear refractive index is $n_2 \approx 5 \times 10^{-20}$ $\text{m}^2 \text{W}^{-1}$ [23]. The resulting estimate of the critical power should be compared with the data given in Table 1 on the maximum power used in different series of measurements of pulses $P_{\text{max}} \approx (1-R)Q_{\text{max}}/\tau$, where R is the reflection coefficient at the air–diamond interface, Q_{max} is the maximum energy of the laser pulse in the series, and τ is the FWHM pulse duration. Obviously, the self-focusing effect may be neglected in experiments with 1- and 5-ps pulses, which allows one to correctly use the technique described above to restore the real energy profile inside the diamond plate. In using a lens with $\text{NA} = 0.36$ the Kerr nonlinearity also should not have a significant impact on the energy profile along the beam axis. However, in the case of a lower numerical aperture of the focusing lens ($\text{NA} = 0.09$) one should

Table 1. Maximum power (kW) in the experimental series.

NA	τ/fs		
	140	1000	5000
0.36	650	250	50
0.09	1300 (400)	400	80

Note: in brackets we present the power needed for the optical breakdown.

expect significant self-focusing of femtosecond pulses, except, perhaps, pulses with a minimal energy that is close to the breakdown threshold of diamond.

4. Calculation of spherical aberrations

The electric field amplitude E at point P on the optical axis inside the diamond plate was determined by numerical calculation of the Fresnel–Kirchhoff diffraction integral [24]:

$$E(P) = \frac{i}{2\lambda} \iint_{\Sigma} E_x(M) \frac{\exp(-ik_2 s)}{s} (\cos\beta + \cos\varphi) d\sigma, \quad (5)$$

where Σ is the integration surface corresponding to the air–diamond interface (Fig. 3); s is the distance from point M on the integration surface to point P; k_2 is the wavenumber in diamond; β is the angle of refraction; and φ is the angle between the segment PM and the z axis. It was assumed that the initial laser beam is linearly (vertically) polarised; therefore, when integrating we took into account only the projection E_x of the electric field vector on the x axis.

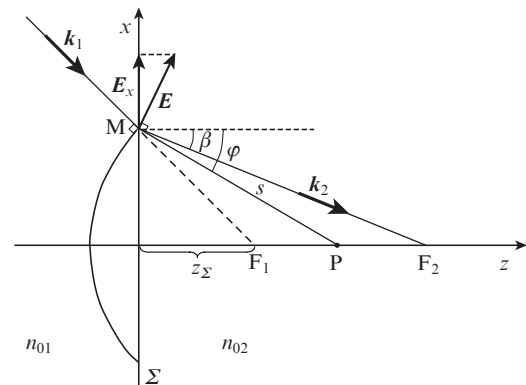


Figure 3. Calculation of the electric field distribution in diamond.

The use of a well-known paraxial approximation for a Gaussian beam in the calculation of the complex electric field amplitude on the integration surface is valid only at a sufficiently low numerical aperture of the focusing lens. Therefore, in the calculation we assumed that a converging spherical wave with a fixed centre and a Gaussian amplitude distribution across the beam cross section is incident on the diamond plate. The condition for the applicability of this approximation is the fulfilment of the relation $z_{\Sigma}^2 \gg z_{f1}^2$, where z_{Σ} is the distance from the surface Σ to the geometrical focal point of the lens F_1 excluding refraction at the air–diamond interface, and z_{f1} is the Rayleigh length of the laser beam waist in the air. Thus, the calculations were performed only for a sufficiently large depth of the focal plane in the diamond plate ($z_{\Sigma} > 10z_{f1}$). The electric field amplitude at point M on the surface Σ was found from the expression

$$E(M) \equiv E(x_M, y_M) = \sqrt{1-R(M)} \times A_L \frac{\mathcal{F}}{z_{\Sigma}} \exp\left(-\frac{x_M^2 + y_M^2}{w_{\Sigma}^2} - ik_1 \sqrt{x_M^2 + y_M^2 + z_{\Sigma}^2}\right), \quad (6)$$

where $R(M)$ is the Fresnel reflection coefficient at point M; A_L is the field amplitude on the optical axis immediately after

the focusing lens; \mathcal{F} is the focal distance of the lens; and k_1 is the wavenumber in air. The Gaussian radius of the amplitude distribution on the surface Σ is given by the formula

$$w_\Sigma = \frac{w_L z_\Sigma}{\mathcal{F}}, \quad (7)$$

where w_L is the Gaussian beam radius on the lens.

Formulas for calculating the remaining quantities (s , $\cos\beta$ and $\cos\varphi$) in integral (5) can be easily derived based on the scheme shown in Fig. 3.

5. Results and discussion

A decrease in the maximum intensity near the focus during a shift of the focal plane inside the sample is one of the most visible and easily experimentally verifiable manifestations of spherical aberrations. The calculated dependences of the maximum intensity at the beam axis on the focusing depth for two values of the numerical aperture used in the experiment are shown in Fig. 4. The maximum intensity in the absence of aberration is taken to be unity. A rapid decrease in the calculated maximum intensity with increasing focusing depth for $\text{NA} = 0.36$ is correlated with the experimentally observed increase in the pulse energy necessary for the optical breakdown of diamond. Based on the fixed threshold intensity for the optical breakdown, it is expected that the quantity, which is inverse to the pulse energy threshold (see Fig. 4), will be proportional to the calculated maximum intensity. This is true if the focusing depth is more than $500 \mu\text{m}$; however, with decreasing burial depth the experimental breakdown threshold varies more slowly than that predicted in the calculations. For $\text{NA} = 0.09$ we failed to observe in the experiment the changes in the breakdown threshold in the depth range of $300\text{--}1700 \mu\text{m}$ with an accuracy up to 7%, which is fully consistent with the results of the calculations: reduction in the maximum intensity at a depth of 2 mm does not exceed 2%.

The effect of the numerical aperture of the focusing lens on spherical aberrations in diamond is shown in Fig. 5. The calculation was performed for several fixed focusing depths, based on the maximum thicknesses of diamond plates that are currently available on the market. It follows from the plotted curves that the use of focusing optics with $\text{NA} < 0.1\text{--}0.2$

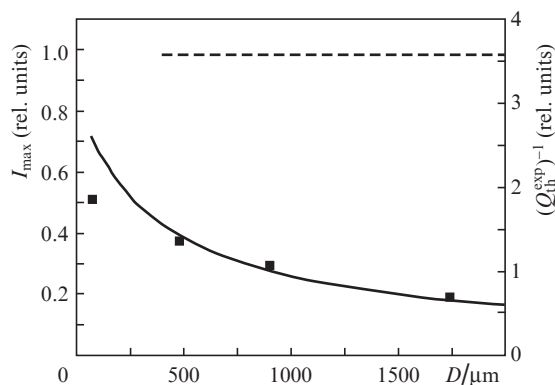


Figure 4. Calculated dependences of the maximum intensity I_{\max} at a beam axis on the focusing depth D for $\text{NA} = 0.36$ (solid curve) and 0.09 (dashed line). The points correspond to the inverse value of the experimental threshold pulse energy $Q_{\text{th}}^{\text{exp}}$ for the optical breakdown of diamond at $\text{NA} = 0.36$.

(depending on the focusing depth) allows one to completely avoid the negative effects of spherical aberration during the microstructuring of diamond. In this case, the minimum diameter of the aberration-free laser caustics in diamond is $\sim 2\lambda/(\pi \cdot \text{NA}) \approx 3\text{--}5 \mu\text{m}$ ($\lambda = 800 \text{ nm}$), which imposes restrictions on the minimum cross section of the fabricated microstructures.

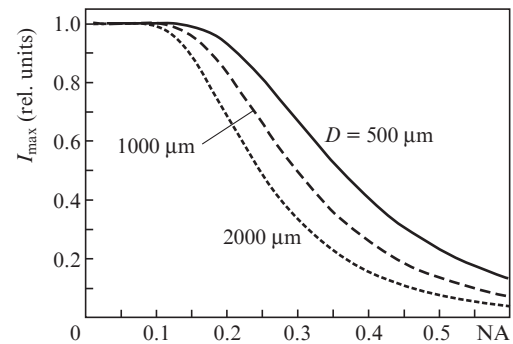


Figure 5. Effect of the numerical aperture of the laser beam on the calculated maximum intensity for several focusing depths D .

Figure 6 shows that the calculated dependences of the laser intensity on the z coordinate are in agreement with real energy profiles recovered in the experiment. Note that all the recovered profiles do not reach the point corresponding to the calculated intensity maximum, forming a gap of about $50 \mu\text{m}$ wide for $\text{NA} = 0.09$, and $5\text{--}12 \mu\text{m}$ for $\text{NA} = 0.36$. The reason is the low reliability of the results of experimental data pro-

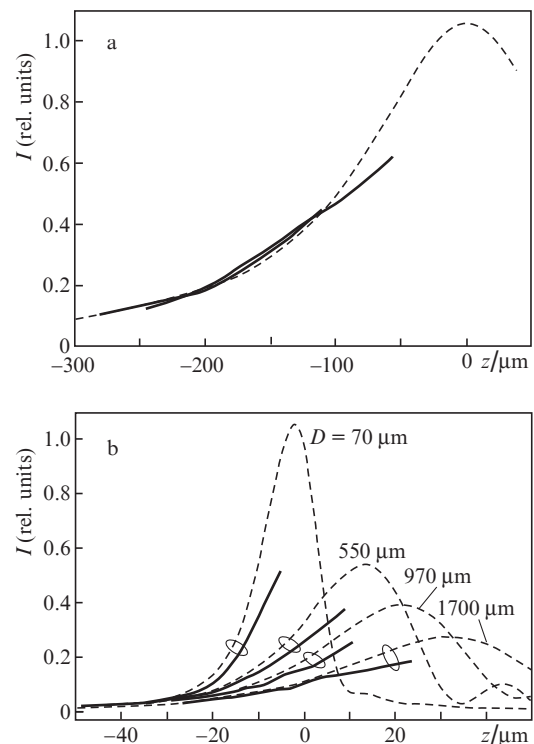


Figure 6. Calculated (dashed curves) and experimental (solid curves) intensity profiles at the beam axis for several focusing depths D ($\tau = 5 \text{ ps}$) with $\text{NA} =$ (a) 0.09 ($D = 300$ and $1700 \mu\text{m}$) and (b) 0.36 .

cessing, associated with a small number of initial measurements of the graphitisation wave velocity in this region. In combination with unpredictable fluctuations of the graphitisation rate from point to point, caused by a specific mechanism of the graphitisation wave propagation [21], a reliable measurement of the averaged component of the dependence $V_{av}(z)$, which is used to recover the energy profile of the beam, becomes impossible.

As was expected (see Fig. 4), for a low numerical aperture lens (NA = 0.09) there is a very good agreement of the experimental intensity profiles for two different focusing depths $D = 300$ and $1700 \mu\text{m}$ (Fig. 6a). The calculated intensity profile for the same D was obtained by formula (2) for a Gaussian beam (deviation from the results found by the Fresnel–Kirchhoff integral is less than 2%). On the other hand, the recovered intensity profiles for a high numerical aperture lens (NA = 0.36) demonstrate a characteristic drop and stretching with increasing penetration depth of the focal plane (Fig. 6b). The experimental profiles reproduce in the general shape of the calculated curves; however, they exhibit a systematic deviation, which increases with approaching the intensity maximum. For a low numerical aperture lens this deviation is not evident and may be due to the low reliability of data averaging near the intensity maximum. However, for a high numerical aperture lens the profiles begin to diverge far from the intensity maximum, and near the intensity maximum corresponding they differ twice (for $D = 70 \mu\text{m}$).

The most likely reason for such a large discrepancy is the aberration of a real laser beam before its penetration into the diamond plate, while in calculations the wavefront shape behind the lens was assumed spherical. Recall that the results of the preliminary research on laser beam focusing in the air (see Section 2) also point to a strong aberration of the beam as it passes through a high numerical aperture lens. If we take into account the fact that the deformation of the energy profile of the beam inside diamond, caused by spherical aberrations on the input face, increases with increasing focusing depth, one should expect a simultaneous decrease in the relative contribution of the spherical aberration of the lens that was neglected in the calculations. Indeed, with increasing focusing depth the difference between the experimental and calculated intensity profiles in Fig. 6b is noticeably less evident. As a result, the intensity maximum decreases slower with depth than would be expected from the calculations. This explains the marked difference in the rates of changes in the inverse breakdown threshold and the calculated intensity maximum for NA = 0.36 in Fig. 4.

Using low numerical aperture optics for focusing a laser beam allows one to avoid the beam deformation due to spherical aberrations and, at the same time, leads to an increase in the minimum pulse energy (or peak power) required for the optical breakdown of the material. As a result, the increased breakdown threshold power can be close to the critical self-focusing power, or even exceed it, which again makes important the issue of the laser beam deformation because of self-focusing. In our experiments, a similar situation occurred in focusing femtosecond pulses by a low numerical aperture lens (NA = 0.09), i.e. the maximum power significantly exceeded the critical self-focusing power although the breakdown threshold power was two times lower (see Table 1). The use of the above techniques of the experimental intensity profile recovery is incorrect in this case, since the laser beam distortion during self-focusing leads to a violation of conditions (4). However, there is an easy way to evaluate the difference

between the real axial intensity profiles for femtosecond and picosecond pulses focused by the same low numerical aperture lens.

The available video recordings of the evolution of the graphitised region in diamond allow us, in particular, to obtain data on the position $z_{br}(Q)$ of the point of the initial breakdown of diamond, which is shifted from the focal plane towards the laser beam with increasing pulse energy. The shift is due to the fact that the breakdown occurs at a point where the local energy density reaches a certain threshold value F_{br} (Fig. 7a). For $\tau = 5$ ps and NA = 0.09 the recovered energy density profile $F(z)$ is close to Gaussian (see Fig. 6a), i.e. described by formula (2), which gives the relationship:

$$z_{br}(Q) = z_{f2} \sqrt{\frac{2Q}{\pi w_0^2 F_{br}} - 1}, \quad (8)$$

where $z_{f2} = \pi n w_0^2 / \lambda$ is the Rayleigh waist length in diamond.

Figure 7b shows the experimental dependence $z_{br}(Q)$ for $\tau = 5$ ps (squares) and its approximation by formula (8) (dashed curve). Also presented are the experimental dependences $z_{br}(Q)$ for femtosecond pulses, the upper scale of the pulse energy range being chosen such that the breakdown thresholds for both pulse durations coincide in the figure. The actual agreement between the experimental dependences $z_{br}(Q)$ for $\tau = 140$ fs and 5 ps (including the spread of the data and different breakdown thresholds F_{br}) means that the axial

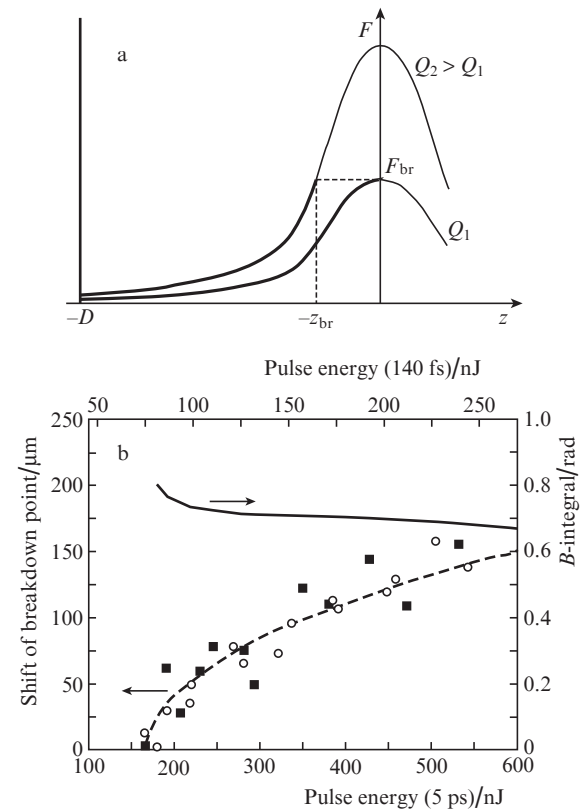


Figure 7. (a) Illustration to the shift of the breakdown point from the focal plane towards the beam with increasing pulse energy, and (b) an experimental shift of the breakdown point for $\tau = 5$ ps (■) and 140 fs (○) and values of the B -integral for $\tau = 140$ fs (solid curve) as a function of the pulse energy at NA = 0.09.

profiles of the energy density $F(z)$ in both cases are very close and described by formula (2). This result, at first sight, is clearly contrary to our assumptions about the intense self-focusing of high-energy femtosecond pulses.

To understand this contradiction, it is necessary to take into account the fact that the process of laser-induced graphitisation of diamond is localised in front of the focal plane in that spatial region where the energy density does not exceed the breakdown threshold. The corresponding part of the energy profile $F(z)$ is shown in Fig. 7a by a thick line. The wavefront distortion in a given plane, which determines the actual occurrence of self-focusing, can be estimated with the help of the B -integral [25], which describes the accumulated change in the phase of the wave on the beam axis due to the Kerr nonlinearity. The integration is performed on a section from the front surface of the diamond sample to the given plane. In the case of a Gaussian beam (i.e. in the absence of a significant transformation of the energy profile) the value of the B -integral at the point of the optical breakdown can be calculated by the formula

$$B(z_{\text{br}}) = \frac{2\pi}{\lambda} \int_{-D}^{-z_{\text{br}}} n_2 I dz$$

$$= \frac{2\pi}{\lambda} n_2 I_0 z_{12} \left[\tan^{-1} \left(\frac{D}{z_{12}} \right) - \tan^{-1} \left(\frac{z_{\text{br}}}{z_{12}} \right) \right], \quad (9)$$

where n_2 is the nonlinear refractive index of diamond, and I_0 is the intensity in the focal plane. Substituting into (9) the experimental data $z_{\text{br}}(Q)$ for $\tau = 140$ fs, approximated by formula (8), we obtained the B -integral as a function of the pulse energy [$B(Q)$ for $D = 300 \mu\text{m}$]. As follows from Fig. 7b, the maximum value of the B -integral at the breakdown point is reached at a minimum pulse energy, sufficient for the optical breakdown of diamond. With increasing pulse energy the B -integral is gradually reduced as the growth of the laser intensity at each point is compensated for by the shortening of the interval of integration due to the withdrawal of the breakdown point of the focal plane.

The obtained integral change of the phase on the beam axis (less than 0.8 rad) from the front face of diamond to the optical breakdown point, i.e. in the region of a potential laser diamond modification, is not sufficient for a visible transformation of the energy profile of the beam despite the fact that the critical self-focusing power is achieved at a femtosecond pulse energy of 137 nJ (the maximum energy is 245 nJ). A significant growth of the B -integral for the high pulse energies is observed only behind the breakdown point (i.e. closer to the focal plane) and does not affect the process of laser microstructuring of diamond. By increasing the focusing depth D from 300 to 1700 μm , the maximum value of the B -integral at the breakdown point for the same pulse energies increases by only 70%, which also should lead to a significant transformation of the energy profile. The presented results of the calculations by the B -integral emphasise an important feature of the self-focusing effect: the wavefront distortion is spatially localised within a relatively small region near the focal plane where the laser intensity reaches maximum values.

The lack of a significant deformation of the beam in the region of diamond graphitisation, found in the experiment and confirmed by the calculations, is caused by the fact that the minimum output power in the optical breakdown of diamond was twice below the critical self-focusing power. An increased energy (power) of the pulse does not lead to defor-

mation of the beam in the graphitisation region due to the progressive shift of this region from the focal plane. However, with approaching the threshold breakdown power to the critical self-focusing power, for example due to a decrease in the numerical aperture of the focusing lens, self-focusing can have a noticeable impact on the microstructuring of diamond. Note that, unlike the spherical aberration discussed above, this effect will weakly depend on the focusing depth.

6. Conclusions

Numerical simulation of the spherical aberration that occurs during refraction of light on the plane front surface of the diamond sample has made it possible to quantitatively assess the laser beam deformation as a function of the focusing depth and numerical aperture of the focusing objective. For a typical diamond sample thickness of 0.5 mm, the maximum change in intensity near the focus point does not exceed 1% when use is made of a focusing lens with a numerical aperture $NA < 0.2$. With increasing sample thickness to 2 mm, which is close to the limiting thickness of commercially available diamond single crystals, the critical value of the numerical aperture is reduced to ~ 0.1 . The simulation results are generally in good agreement with the experimental data on the axial profile of the laser intensity inside diamond in front of the focal plane, recovered using original techniques using the correlation between the local intensity and the average velocity of the graphitisation wave propagation. The observed discrepancies are apparently due to the undocumented aberration of the laser beam as it passes through an aspherical, high numerical aperture lens.

We have found that, in considering the impact of the self-focusing effect on the laser beam deformation during diamond microstructuring, one should take into account the fact that the laser modification of the material occurs in front of the focal plane, the distance from the graphitisation zone to the plane increasing with increasing pulse energy. The calculation of the B -integral characterising the beam wavefront distortion due to self-focusing shows that if the beam deformation is absent at a minimum pulse energy that causes a breakdown of diamond, a further increase in the pulse energy will also not lead to the transformation of the energy beam profile in the graphitisation region.

Acknowledgements. This work was supported by the Russian Foundation for Basic Research (Grant No. 13-02-12068).

References

1. Miura K., Qiu J., Inouye H., Mitsuyu T., Hirao K. *Appl. Phys. Lett.*, **71**, 3329 (1997).
2. Homoelle D., Wielandy S., Gaeta A.L., Borrelli N.F., Smith C. *Opt. Lett.*, **24**, 1311 (1999).
3. Streltsov A.M., Borrelli N.F. *Opt. Lett.*, **26**, 42 (2001).
4. Della Valle G., Taccheo S., Osellame R., Festa A., Cerullo G., Laporta P. *Opt. Express*, **15**, 3190 (2007).
5. Marcinkevičius A., Juodkazis S., Watanabe M., Miwa M., Matsuo S., Misawa H., Nishii J. *Opt. Lett.*, **26**, 277 (2001).
6. Török P., Varga P., Laczik Z., Booker G.R. *J. Opt. Soc. Am. A*, **12**, 325 (1995).
7. Wiersma S.H., Török P., Visser T.D., Varga P. *J. Opt. Soc. Am. A*, **14**, 1482 (1997).
8. Marcinkevičius A., Mizeikis V., Juodkazis S., Matsuo S., Misawa H. *Appl. Phys. A*, **76**, 257 (2003).
9. Liu D., Li Y., An R., Dou Y., Yang H., Gong Q. *Appl. Phys. A*, **84**, 257 (2006).

10. Hnatovsky C., Taylor R.S., Simova E., Bhardwaj V.R., Rayner D.M., Corkum P.B. *J. Appl. Phys.*, **98**, 013517 (2005).
11. Diez-Blanco V., Siegel J., Ferrer A., Ruiz de la Cruz A., Solis J. *Appl. Phys. Lett.*, **91**, 051104 (2007).
12. Kononenko T.V., Meier M., Komlenok M.S., Pimenov S.M., Romano V., Pashinin V.P., Konov V.I. *Appl. Phys. A*, **90**, 645 (2008).
13. Shimizu M., Shimotsuma Y., Sakakura M., Yuasa T., Homma H., Minowa Y., Tanaka K., Miura K., Hirao K. *Opt. Express*, **17**, 46 (2009).
14. Kononenko T.V., Konov V.I., Pimenov S.M., Rossukanyi N.M., Rukovichnikov A.I., Romano V. *Diamond Relat. Mater.*, **20**, 264 (2011).
15. Simmonds R.D., Salter P.S., Jesacher A., Booth M.J. *Opt. Express*, **19**, 24122 (2011).
16. Caylar B., Pomorski M., Bergonzo P. *Appl. Phys. Lett.*, **103**, 043504 (2013).
17. Lagomarsino S., Bellini M., Corsi C., Gorelli F., Parrini G., Santoro M., Sciortino S. *Appl. Phys. Lett.*, **103**, 233507 (2013).
18. Kononenko T., Ralchenko V., Bolshakov A., Konov V., Allegrini P., Pacilli M., Conte G., Spiriti E. *Appl. Phys. A*, **114**, 297 (2014).
19. Kononenko T.V., Dyachenko P.N., Konov V.I. *Opt. Lett.*, **39**, 6962 (2014).
20. Sun B., Salter P.S., Booth M.J. *Appl. Phys. Lett.*, **105**, 231105 (2014).
21. Kononenko T.V., Zavedeev E.V., Kononenko V.V., Ashikkalieva K.K., Konov V.I. *Appl. Phys. A*, **119**, 405 (2015).
22. Fibich G., Gaeta A.L. *Opt. Lett.*, **25**, 335 (2000).
23. Mildren R.P., in *Optical Engineering of Diamond* (Chichester: Wiley, 2013) pp 1–34.
24. Born M., Wolf E. *Principles of Optics* (London: Pergamon Press, 1970; Moscow: Nauka, 1970).
25. Couairon A., Mysyrowicz A. *Phys. Rep.*, **441**, 47 (2007).